CrossMark

ARTICLE

Green-chemistry Compatible Approach to TiO$_2$-supported PdAu Bimetallic Nanoparticles for Solvent-free 1-Phenylethanol Oxidation under Mild Conditions

Jian-Bing Chang · Chang-Hai Liu · Jie Liu · Yu-Yan Zhou · Xu Gao · Sui-Dong Wang

Abstract TiO$_2$-supported PdAu bimetallic nanoparticles (NPs) with small size and good dispersity were prepared by the room-temperature ionic liquid-assisted bimetal sputtering, which is simple, environmentally friendly, and free of additives and byproducts. Pd/Au atomic ratio can be tuned by controlling the sputtering conditions simply. High catalytic activity was found in PdAu–NPs–TiO$_2$ hybrids for solvent-free selective oxidation of 1-phenylethanol using O$_2$ as the oxidant at the low temperature of 50 °C and low pressure of 1 atm. It was found that Pd/Au ratio strongly affected the catalytical activity, and the highest conversion of about 35 % and turnover frequency of about 421 h^{-1} were achieved at 1:1 of Pd/Au atomic ratio. The synergistic effect in PdAu NPs was also discussed based on the comprehensive characterization results. The present approach may offer an alternative platform for future development of green-chemistry compatible bimetallic nanocatalysts.

Keywords PdAu nanoparticles · TiO$_2$ nanosupport · Electronic structure

1 Introduction

The selective oxidation of primary alcohols to aldehydes/ketones is crucially important in both laboratory and commercial processes [1–4]. In homogeneous catalysis for conversion of alcohols to aldehydes, it is often needed to use organic solvents, which are typically expensive, toxic, and harmful to the environment [5]. Thus, great efforts have been made to design and synthesize alternative catalysts which can use molecular O$_2$ as the oxidant. However, the use of O$_2$ under severe conditions such as high temperature and high pressure could induce issues of overoxidation, decomposition products, and/or explosion risk. It is hence highly desired to realize the efficient

catalysis free of solvents under mild conditions. Toward this target, metal nanoparticles (NPs) such as Au NPs [6–15], Pd NPs [16, 17] and PdAu bimetallic NPs [18–24] have been demonstrated to be promising catalysts for solvent-free selective oxidation of alcohols [8, 10, 11, 20, 21]. Especially, PdAu bimetallic NPs often exhibit superior catalytic performance than their monometallic counterparts due to the synergistic effects [18–24]. In order to maintain the small size and good dispersion of PdAu NPs, which are beneficial for the catalysis, nanosupports have been extensively utilized to stabilize the bimetallic NPs on top.

The conventional way to synthesize supported metal NPs involves reduction of corresponding metal salts, where additives such as capping agents and byproducts are always present [25–28]. In some cases, high-temperature processing is required as well [29, 30]. Recently, we have developed a more environmentally friendly strategy using the room-temperature ionic liquid (RTIL)-assisted sputtering to prepare supported metal NPs [31, 32], which is simple, clean, and totally free of additives and byproducts. By the green-chemistry compatible method, PdAu NPs are successfully decorated on TiO$_2$ NPs which act as the

J.-B. Chang · C.-H. Liu · J. Liu · Y.-Y. Zhou · X. Gao · S.-D. Wang (✉)
Soochow University-Western University Joint Centre for Synchrotron Radiation Research, Jiangsu Key Laboratory for Carbon-Based Functional Materials & Devices, Institute of Functional Nano & Soft Materials (FUNSOM), Soochow University, Suzhou 215123, Jiangsu, People's Republic of China
e-mail: wangsd@suda.edu.cn

308

Nano-Micro Lett. (2015) 7(3):307–315

nanosupport. The comprehensive results demonstrate the bimetallic nature of the PdAu NPs, and charge redistribution is observed among Pd, Au, and TiO$_2$. The TiO$_2$-supported bimetallic NPs show good catalytic capability for the selective oxidation reaction of 1-phenylethanol to acetophenone, which can occur near room temperature without a solvent. Furthermore, the catalytic activity of the PdAu NPs is significantly dependent on Pd/Au ratio, suggesting a strong correlation among the catalytic performance, bimetallic composition, and charge redistribution.

2 Experimental

2.1 Materials

Pd and Au targets for the sputtering were purchased from Hefei Kejing. 1-phenylethanol was purchased from Sinopharm Chemical Reagent. Pristine TiO$_2$ NPs with an average diameter of 25 nm were acquired from Hangzhou Wanjing. The RTIL, 1-Butyl-3-methylimidazolium tetrafluoroborate ([BMIm][BF$_4$], purity >99 %), was purchased from Shanghai Chengjie Chemical, which was dried in vacuum for 24 h before use.

2.2 Synthesis of TiO$_2$-supported PdAu NPs

As depicted in Scheme 1, the TiO$_2$-supported PdAu NPs were prepared by successive sputtering of Au and Pd onto the TiO$_2$–RTIL suspension [31, 32]. Firstly, 10 mg TiO$_2$ NPs were adequately dispersed into 10 mL [BMIm][BF$_4$] with ultrasonication. Secondly, the TiO$_2$–RTIL suspension was dropped into a clean stainless steel pot, and then Au was sputtered onto the suspension at room temperature in a desktop sputtering system (Quorum Technologies, equipped with a thickness monitor which is pre-calibrated by a surface profiler). Thirdly, Pd was sputtered onto the Au–TiO$_2$–RTIL suspension by simply altering the metal target from Au to Pd. During the sputtering, Ar working pressure
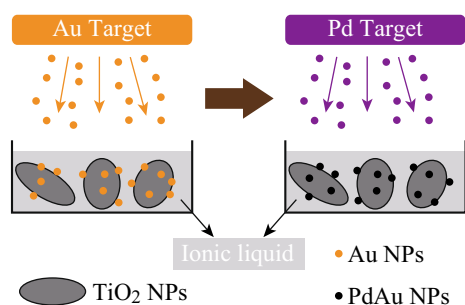
Scheme 1 Preparation method for PdAu–NPs–TiO$_2$ hybrids: Successive sputtering of Au and Pd onto RTIL of [BMIm][BF$_4$], in which TiO$_2$ NPs are pre-dispersed

and deposition rate were kept at about 0.01 mbar and 0.2 Å s^{-1}, respectively. The total sputtering time was controlled to be same for all the samples to get a same metal loading, e.g., 40 s for Au plus 40 s for Pd to the PdAu bimetallic NPs, and correspondingly 80 s for Au/Pd to the monometallic NPs. Eventually, the metal–NP–TiO$_2$ hybrids were separated from [BMIm][BF$_4$] by repeated high-speed centrifugation and decantation. Note that the current approach is a general method, which can be used to prepare various bimetallic NPs on diverse nanosupports [31, 32].

2.3 Characterization of TiO$_2$-supported PdAu NPs

The crystalline structures of the metal–NPs–TiO$_2$ hybrids were characterized with X-ray diffraction (XRD, PANalytical Empyrean) with Cu $K\alpha$ radiation. The microscopic structures of the metal–NPs–TiO$_2$ hybrids were investigated with high-resolution transmission electron microscopy (HRTEM, FEI Quanta FRG 200F, operating at 200 kV) and high-angle annular dark-field scanning transmission electron microscopy (HAADF-STEM). The UV–Vis absorption measurements were carried out on a UV–Vis–NIR spectrophotometer (PerkinElmer, Lambda 750). The electronic structures of the metal–NPs–TiO$_2$ hybrids were characterized with X-ray photo-emission spectroscopy (XPS, Kratos Axis Ultra DLD, monochromatic Al $K\alpha$). The X-ray absorption near-edge structure (XANES) measurements were performed at the BL14W1 beamline of the Shanghai Synchrotron Radiation Facility (SSRF).

2.4 Catalytic Reaction with TiO$_2$-supported PdAu NPs

The solvent-free oxidation reaction of 1-phenylethanol using O$_2$ was conducted in a glass flask pre-filled with 5 mL 1-phenylethanol and 8 mg hybrid catalyst. The mixture was stirred and heated using a magnetic stirrer with heating function. The system was equipped with a thermocouple to control the temperature and a reflux condenser to recover the vaporized solution. In each reaction run, the mixture was raised to 50 °C under stirring (1000 rpm). O$_2$ was bubbled into the mixture at a constant flow rate (250 mL min^{-1}) to initiate the reaction. After the reaction lasting 5 h, the reaction products were quantitatively analyzed with gas chromatograph (GC, Agilent).

The conversion, selectivity, and turnover frequency (TOF) are defined as follows:

$$\text{Conversion (\%)} = \frac{\text{mol of reactant converted}}{\text{mol of reactant in feed}} \times 100\%$$

$$\text{Selectivity (\%)} = \frac{\text{mol of target formed}}{\text{mol of reactant converted}} \times 100\%$$

$$TOF\ \left(h^{-1}\right) = \frac{\text{mol of reactant converted}}{\left(\text{mol of total metal}\right) D_m t}$$

where the amount of reactant and target product are measured by GC; the amount of total metal are approximated as the amount of Au and Pd atoms, which are measured by inductively coupled plasma atomic emission spectroscopy (ICP-AES); D_m is the dispersivity of metal; and t is the reaction time.

3 Results and Discussion

3.1 Microscopic Structure

Commercially available TiO_2 NPs with an average diameter of 25 nm were used as the nanosupport, and the morphology is shown in Fig. 1a. Utilizing the RTIL-assisted sputtering method, Au/Pd monometallic NPs or PdAu bimetallic NPs were decorated on the TiO_2 support, where Pd/Au ratio (atomic ratio, unless otherwise noted) was controlled by adjusting the sputtering conditions of Au and Pd [32]. It was noted that the TiO_2 support played a role of stabilizing metal NPs on top, otherwise the metal NPs will aggregate in cleaning process for removing [BMIm][BF_4] if the support is absent [31]. Figure 1b–f displays the TEM images and metal nanoparticle size distributions of the Au–TiO_2, PdAu (1:4)–TiO_2, PdAu (1:1)–TiO_2, PdAu (4:1)–TiO_2, and Pd–TiO_2 hybrids, respectively. It can be seen that the size of Au monometallic NPs is larger than that of Pd monometallic NPs, and the size of PdAu bimetallic NPs decreases gradually from about 5 to 3 nm upon increasing Pd/Au ratio.

In order to clarify the microscopic structure of PdAu NPs, the elemental spatial distribution of Au and Pd is probed by mapping of the energy-dispersive spectroscopy (EDS). Figure 2a–d illustrates the HAADF-STEM images for the sample of PdAu (1:1)–TiO_2, where Au and Pd spatial distributions are almost overlapped with each other. Similar HAADF-STEM results were observed for the samples with other Pd/Au ratios, and it suggests that Au and Pd are intermixed in the PdAu NPs due to atomic interdiffusion [33–37]. The strong intermixing of Au and Pd can provide a large number of Au/Pd interfaces, which may be in favor of promoting catalytic activity of PdAu NPs [38]. On the other hand, the Ti and O spatial distributions are consistently uniform, as demonstrated in Fig. 2e, f.

Figure 3 shows the UV–Vis absorption spectra of the TiO_2-supported metal NPs with different Pd/Au ratios, in which the surface plasmon resonance (SPR) band of Au is around 570 nm. There is a small red-shift compared with the SPR band of typical Au NPs (~ 530 nm), which could be caused by the electronic structure modification of Au

NPs due to the electron transfer from TiO_2 to Au [39–43]. Upon addition of Pd, the SPR band gradually disappears. The disappearance of the SPR feature supports the HAADF-STEM-derived claim that Au and Pd are intermixed in the PdAu NPs. Therefore, the PdAu NPs are concluded to be bimetallic NPs rather than a physical mixture of separate Au and Pd monometallic NPs.

3.2 Electronic Structure

The charge redistribution in PdAu NPs is another bimetallic signature, which is investigated by XPS and XANES based on synchrotron radiation. Figure 4a shows the XPS Au $4f$ spectra, where the binding energy of Au $4f_{7/2}$ peak for Au monometallic NPs is at about 83.0 eV. Considering the binding energy of bulk Au $4f_{7/2}$ peak (typically at about 84.0 eV), there is a significant negative shift in binding energy (corresponding to electron gaining) for the Au NPs on TiO_2. As TiO_2 NPs often show n-type behavior arising from the oxygen vacancies, electron transfer from the TiO_2 support to the Au NPs may be responsible for the binding energy shift [44]. Upon addition of Pd, the Au $4f$ peaks are further negatively shifted (up to 0.3 eV) with increasing Pd/Au ratio. It implies a strong interaction between Au and Pd [39, 44, 45], and electron transfer from Pd to Au may occur and result in a negative shift in binding energy. Furthermore, when Pd/Au ratio is increased, the full width at half maximum (FWHM) of the Au $4f$ peaks is broadened. This can be attributed to the size reduction of PdAu NPs with increasing Pd/Au ratio, as shown in Fig. 1.

Figure 4b shows the XANES Au L_3-edge spectra of the TiO_2-supported metal NPs with different Pd/Au ratios, where the absorption jump (whiteline) region around 11,925 eV is magnified as the inset. The whiteline characterizes the dipole transition from Au $2p$ to $5d$ orbitals, and thus its intensity corresponds to the number of Au d-band holes. Compared with Au monometallic NPs, the whiteline intensity is decreased for PdAu bimetallic NPs, and the sample with higher Pd/Au ratio shows lower whiteline intensity. The trend of the whiteline change may be due to electron transfer from Pd to Au, which is in accordance with the XPS Au $4f$ results and literature [46].

On the other hand, the XPS Pd $3d$ spectra of the TiO_2-supported metal NPs with different Pd/Au ratios are shown in Fig. 4c. The binding energy of Pd $3d_{3/2}$ peak for Pd monometallic NPs is at about 339.8 eV, which is lower than that of bulk Pd at about 340.4 eV. Similar to the Au NPs on TiO_2, the negative shift in binding energy can be ascribed to electron transfer from the n-type TiO_2 support to the Pd NPs. Upon addition and promotion of Au, the original Pd feature is gradually weakened, and a new Pd feature at lower binding energy emerges and grows up. This could be a result of strong interaction between Au and

310

Nano-Micro Lett. (2015) 7(3):307–315
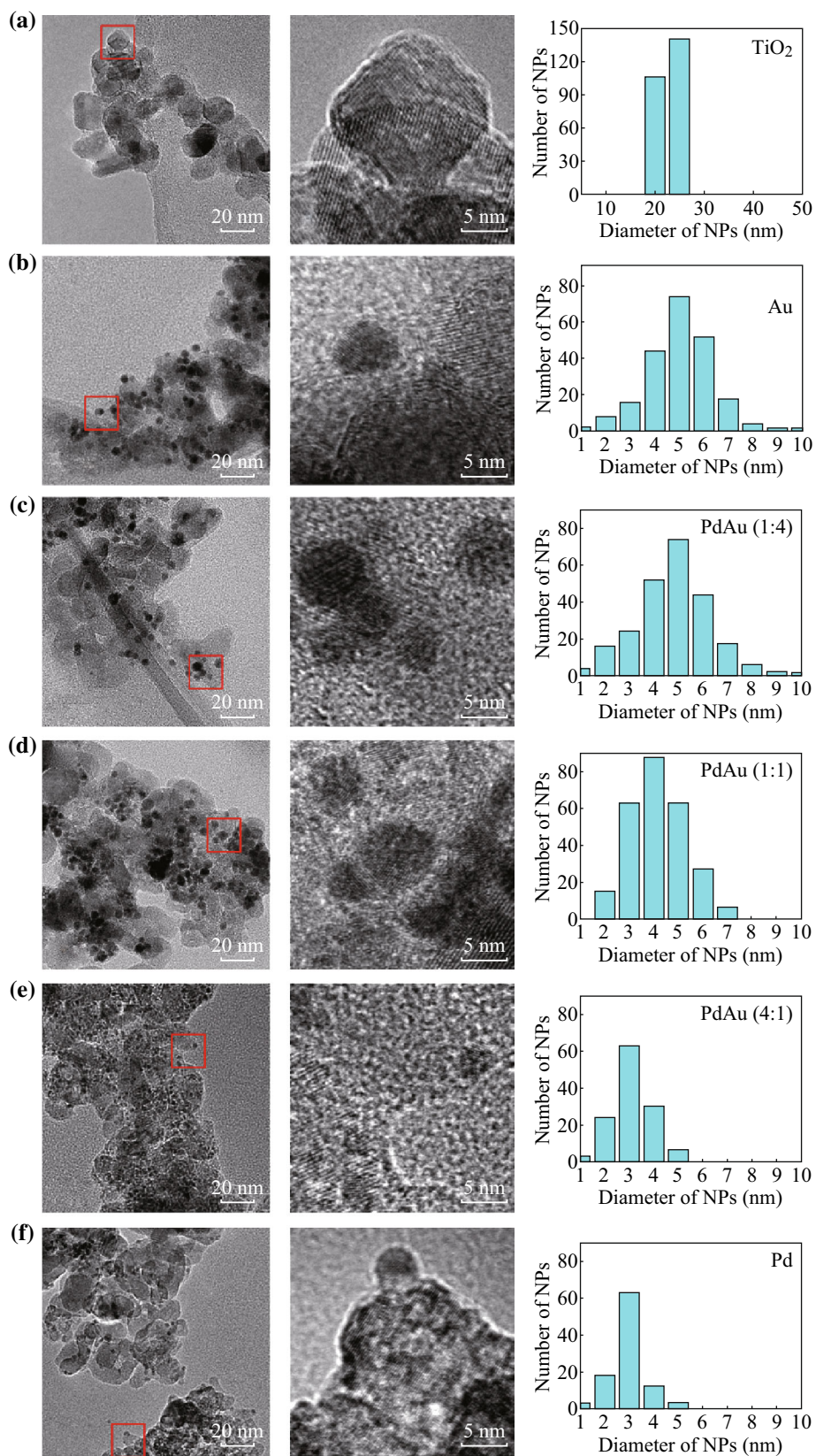
Fig. 1 TEM images and NPs size distributions of **a** TiO$_2$ NPs as the support, **b** Au NPs on TiO$_2$, **c** PdAu (1:4) NPs on TiO$_2$, **d** PdAu (1:1) NPs on TiO$_2$, **e** PdAu (4:1) NPs on TiO$_2$, and **f** Pd NPs on TiO$_2$. TEM images in the *middle* are magnified *square region* shown in the *left*
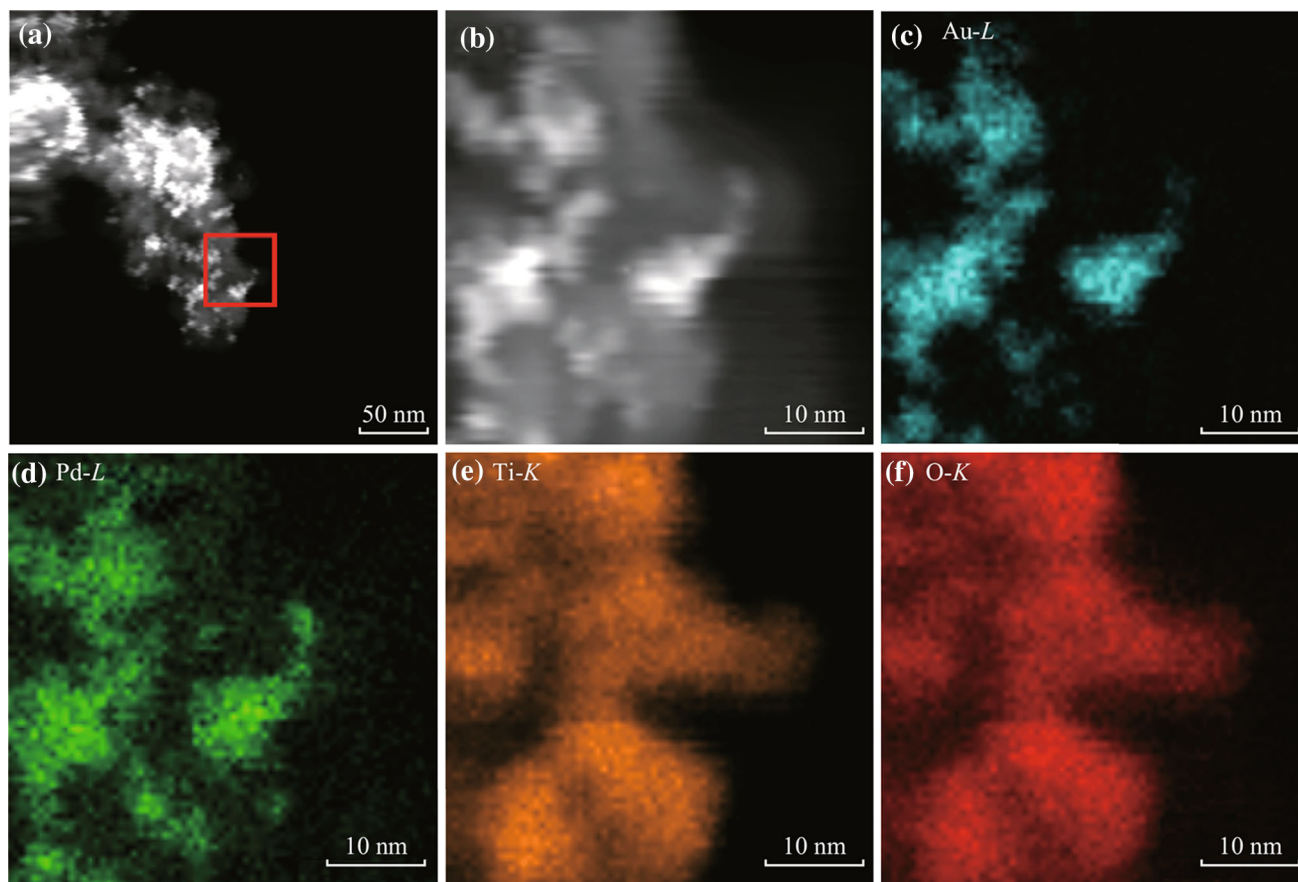
Fig. 2 HAADF-STEM images of PdAu (1:1) NPs on TiO₂ **a** in *large scale* and **b** in selective *small scale*. Elemental mapping for **c** Au, **d** Pd, **e** Ti, and **f** O
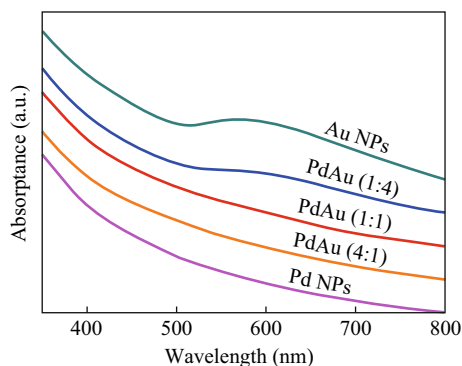
Fig. 3 UV–Vis absorption spectra of TiO₂-supported metal NPs with different Pd/Au atomic ratios

3.3 Crystalline Structure

The XRD patterns of the metal–NPs–TiO₂ hybrids are shown in Fig. 5. The TiO₂ support shows the crystalline features of anatase phase, which remains identical 2θ positions in the hybrids. Thus, there is no phase change or crystallinity degradation of TiO₂ after the metal NPs decoration. For monometallic NPs, the Au diffraction peaks are relatively sharp, whereas the Pd ones are broad or even absent. It is owing to the small size and resultant crystalline defects of the Pd NPs compared with the Au NPs [48, 49], which is consistent with the TEM results. Significantly, the Au diffraction peaks are slightly shifted toward larger 2θ side upon addition of Pd, and the Pd diffraction peaks gradually vanish upon the addition of Au. Both indicate the formation of PdAu bimetallic NPs rather than separate Au/Pd monometallic NPs, in good agreement with the above discussion based on the microscopic and electronic characterization results.

Pd as observed in PdAu alloys [33, 45]. According to the above, the charge redistribution is present in the PdAu NPs, plausibly Pd losing *s*, *p*-electrons and getting *d*-electrons with net electron loss, while Au gaining net *d*-electrons [33, 43, 44, 46, 47].
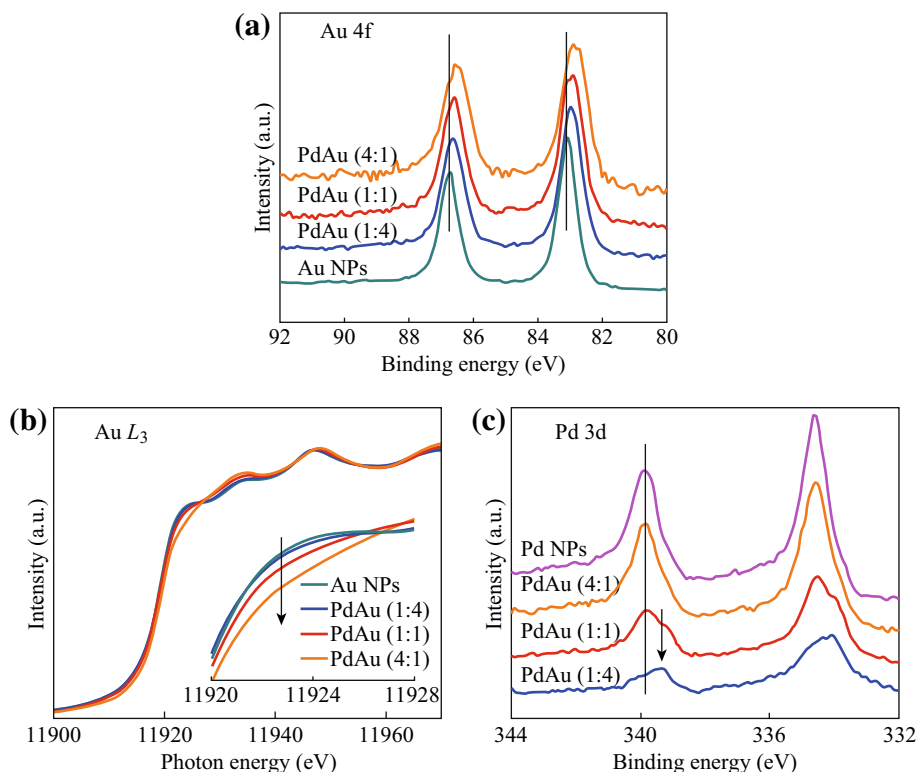
Fig. 4 **a** XPS Au 4*f* spectra, **b** XANES Au *L*₃-edge spectra, and **c** XPS Pd 3*d* spectra of TiO₂-supported metal NPs with different Pd/Au atomic ratios. *Inset* in **b** is magnified *whiteline region*, where Au *L*₃-edge jump is normalized
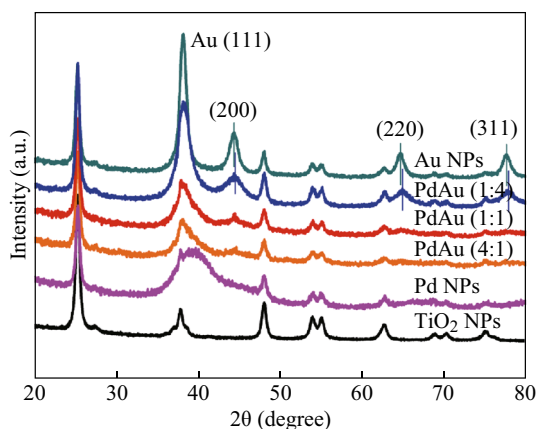
Fig. 5 XRD patterns of TiO₂ NPs (anatase) and TiO₂-supported metal NPs with different Pd/Au atomic ratios

3.4 Catalytic Behavior

Utilizing the present RTIL-assisted sputtering method, PdAu bimetallic NPs on TiO₂ with small size, bare surface, and controlled Pd/Au ratio are achieved. The catalytic activity for 1-phenylethanol oxidation of the metal–NPs–TiO₂ hybrids is systematically studied, and the conversion and selectivity results are shown in Fig. 6a. Note that the catalytic reaction is realized using O₂ as the oxidant at
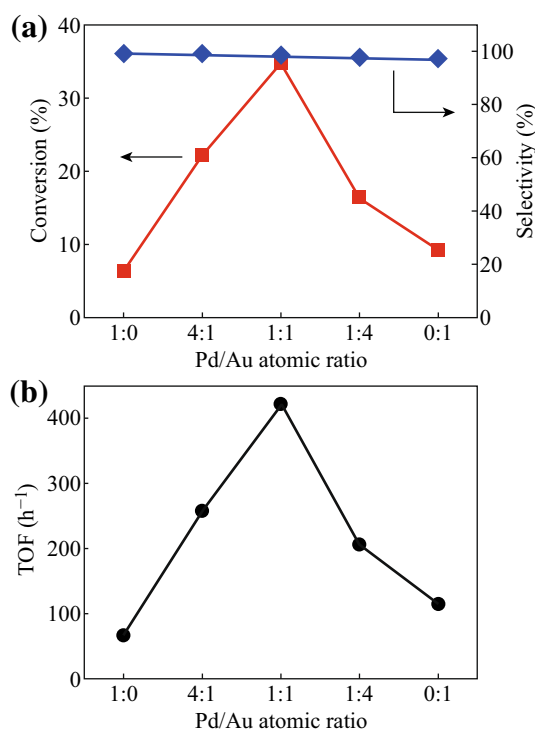
Fig. 6 Dependences of catalytic activity for 1-phenylethanol oxidation on Pd/Au atomic ratio in TiO₂-supported metal NPs: **a** conversion (*square*) and selectivity (*diamond*); **b** turnover frequency (*circle*). The catalytic reaction is carried out at 323 K and 1 atm using O₂ as the oxidant

temperature as low as 50 °C and pressure as low as 1 atm. Furthermore, for a reliable comparison in catalytic activity, the total amount of sputtered metal is controlled to be the same for all the hybrids. Firstly, the Au monometallic NPs appear to be more active than the Pd monometallic NPs. Secondly, all the PdAu bimetallic NPs show higher activity compared with the monometallic counterparts. Thirdly, the conversion from 1-phenylethanol to acetophenone is strongly dependent on Pd/Au ratio, and it gets a maximum of about 35 % at 1:1 Pd/Au ratio. As a more catalytically relevant parameter, the highest TOF of $\sim$421 h^{-1} is obtained at 1:1 Pd/Au ratio as well (Fig. 6b). Finally, the selectivity remains high irrespective of Pd/Au ratio.

The catalytic results suggest that the surface Au diluted by Pd is the active sites, and the synergistic effect can be understood in the following. On one hand, the size of the metal NPs is reduced with increasing Pd/Au ratio, which induces more surface area for the catalytic reaction. Furthermore, the dilution of Au by Pd generates more Au/Pd interface and isolated Au surface, which can promote the catalytic activity of Au (ensemble effect) [38, 50–52]. On the other hand, when Pd/Au ratio is high enough, the number of the Au active sites may decrease. In addition, owing to the charge redistribution effect in PdAu NPs, the d-hole depletion of Au is enhanced with increasing Pd/Au ratio. It may weaken the reactant adsorption on Au, which is adverse to the oxidation catalysis. As a consequence, the combined action of the above promotion and suppression effects shows the highest activity at 1:1 Pd/Au. The synergistic behavior indicates that Pd/Au ratio in PdAu NPs can be well tailored by the present means to optimize their catalytic performance.

4 Conclusion

A green-chemistry compatible approach toward functional PdAu–NPs–TiO$_2$ hybrids is demonstrated, and the hybrids show high catalytic activity for solvent-free synthesis of acetophenone from 1-phenylethanol. The catalytic reaction is realized under mild conditions, using O$_2$ as the oxidant at the low temperature of 50 °C and low pressure of 1 atm. The approach for the catalyst preparation is straightforward and totally free of additives and byproducts. All the microscopic structure, electronic structure, and crystalline structure characterizations indicate the bimetallic formation of the TiO$_2$-supported PdAu NPs due to atomic interdiffusion. The catalytic activity of the PdAu NPs exhibits a strong dependence on Pd/Au ratio, which is tunable using the present RTIL-assisted sputtering method.

References

1. A. Abad, C. Almela, A. Corma, H. García, Efficient chemoselective alcohol oxidation using oxygen as oxidant. Superior performance of gold over palladium catalysts. Tetrahedron **62**(28), 6666–6672 (2006). doi:10.1016/j.tet.2006.01.118
2. K. Zaw, M. Lautens, P.M. Henry, Novel parallel path mechanism for the oxidation of allyl alcohol by aqueous palladium (ii) chloride. Organometallics **2**(1), 197–199 (1983). doi:10.1021/om00073a051
3. D.G. Lee, U.A. Spitzer, Aqueous dichromate oxidation of primary alcohols. J. Org. Chem. **35**(10), 3589–3590 (1970). doi:10.1021/jo00835a101
4. P.V. Prabhakaran, S. Venkatachalam, K.N. Ninan, Permanganate ion supported over crosslinked polyvinylamine as an oxidising agent for alcohols. Eur. Poly. J. **35**(9), 1743–1746 (1999). doi:10.1016/s0014-3057(98)00246-8
5. J. Muzart, Palladium-catalysed oxidation of primary and secondary alcohols. Tetrahedron **59**(31), 5789–5816 (2003). doi:10.1016/s0040-4020(03)00866-4
6. I. Prati, M. Rossi, Gold on carbon as a new catalyst for selective liquid phase oxidation of diols. J. Catal. **176**(2), 552–560 (1998). doi:10.1006/jcat.1998.2078
7. D. Enache, D. Knight, G. Hutchings, Solvent-free oxidation of primary alcohols to aldehydes using supported gold catalysts. Catal. Lett. **103**(1–2), 43–52 (2005). doi:10.1007/s10562-005-6501-y
8. H. Tsunoyama, H. Sakurai, Y. Negishi, T. Tsukuda, Size-specific catalytic activity of polymer-stabilized gold nanoclusters for aerobic alcohol oxidation in water. JACS **127**(26), 9374–9375 (2005). doi:10.1021/ja052161e
9. A. Abad, C. Almela, A. Corma, H. Garcia, Unique gold chemoselectivity for the aerobic oxidation of allylic alcohols. Chem. Commun. **30**, 3178–3180 (2006). doi:10.1039/b606257a
10. H. Tsunoyama, T. Tsukuda, H. Sakurai, Synthetic application of pvp-stabilized au nanocluster catalyst to aerobic oxidation of alcohols in aqueous solution under ambient conditions. Chem. Lett. **36**(2), 212–213 (2007). doi:10.1246/cl.2007.212
11. H. Li, B. Guan, W. Wang, D. Xing, Z. Fang, X. Wan, L. Yang, Z. Shi, Aerobic oxidation of alcohol in aqueous solution catalyzed by gold. Tetrahedron **63**(35), 8430–8434 (2007). doi:10.1016/j.tet.2007.05.117
12. J. Hu, L. Chen, K. Zhu, A. Suchopar, R. Richards, Aerobic oxidation of alcohols catalyzed by gold nano-particles confined in the walls of mesoporous silica. Catal. Today **122**(3–4), 277–283 (2007). doi:10.1016/j.cattod.2007.01.012
13. H. Tsunoyama, N. Ichikuni, H. Sakurai, T. Tsukuda, Effect of electronic structures of Au clusters stabilized by poly(n-vinyl-2-pyrrolidone) on aerobic oxidation catalysis. JACS **131**(20), 7086–7093 (2009). doi:10.1021/ja810045y

314

Nano-Micro Lett. (2015) 7(3):307–315

14. O. Casanova, S. Iborra, A. Corma, Biomass into chemicals: one pot-base free oxidative esterification of 5-hydroxymethyl-2-fur-fural into 2,5-dimethylfuroate with gold on nanoparticulated ceria. J. Catal. 265(1), 109–116 (2009). doi:10.1016/j.jcat.2009.04.019

15. H. Liu, Y. Liu, Y. Li, Z. Tang, H. Jiang, Metal–organic frame-work supported gold nanoparticles as a highly active heteroge-neous catalyst for aerobic oxidation of alcohols. J. Phys. Chem. C 114(31), 13362–13369 (2010). doi:10.1021/jp105666f

16. M. Mifsud, K.V. Parkhomenko, I.W.C.E. Arends, R.A. Sheldon, Pd nanoparticles as catalysts for green, sustainable oxidation of functionalized alcohols in aqueous media. Tetrahedron 66(5), 1040–1044 (2010). doi:10.1016/j.tet.2009.11.007

17. Z. Ma, H. Yang, Y. Qin, Y. Hao, G. Li, Palladium nanoparticles confined in the nanocages of sba-16: enhanced recyclability for the aerobic oxidation of alcohols in water. J. Mol. Catal. A: Chem. 331(1–2), 78–85 (2010)

18. D.I. Enache, J.K. Edwards, P. Landon, B. Solsona-espriu, A.F. Carley, A.A. Herzing, M. Watanabe, C.J. Kiely, D.W. Knight, G.J. Hutchings, Solvent-free oxidation of primary alcohols to aldehydes using Au–Pd/TiO2 catalysts. Science 311(5759), 362–365 (2006). doi:10.1126/science.1120560

19. N. Dimitratos, J. Lopez-sanchez, D. Lennon, F. Porta, L. Prati, A. Villa, Effect of particle size on monometallic and bimetallic (Au, Pd)/c on the liquid phase oxidation of glycerol. Catal. Lett. 108(3–4), 147–153 (2006). doi:10.1007/s10562-006-0036-8

20. W. Hou, N.A. Dehm, R.W.J. Scott, Alcohol oxidations in aque-ous solutions using Au, Pd, and bimetallic AuPd nanoparticle catalysts. J. Catal. 253(1), 22–27 (2008). doi:10.1016/j.jcat.2007.10.025

21. A. Villa, N. Janjic, P. Spontoni, D. Wang, D.S. Su, L. Prati, Au–Pd/AC as catalysts for alcohol oxidation: effect of reaction pa-rameters on catalytic activity and selectivity. Appl. Catal. A: Gen. 364(1–2), 221–228 (2009). doi:10.1016/j.apcata.2009.05.059

22. S. Marx, A. Baiker, Beneficial interaction of gold and palladium in bimetallic catalysts for the selective oxidation of benzyl al-cohol. J. Phys. Chem. C 113(15), 6191–6201 (2009). doi:10.1021/jp808362m

23. A.J. Frank, J. Rawski, K.E. Maly, V. Kitaev, Environmentally benign aqueous oxidative catalysis using AuPd/TiO2 colloidal nanoparticle system stabilized in absence of organic ligands. Green Chem. 12(9), 1615–1622 (2010). doi:10.1039/c0gc00084a

24. Y. Chen, H. Lim, Q. Tang, Y. Gao, T. Sun, Q. Yan, Y. Yang, Solvent-free aerobic oxidation of benzyl alcohol over Pd monometallic and Au–Pd bimetallic catalysts supported on SBA-16 mesoporous molecular sieves. Appl. Catal. A: Gen. 380(1–2), 55–65 (2010). doi:10.1016/j.apcata.2010.03.026

25. J. Gong, C.B. Mullins, Surface science investigations of oxidative chemistry on gold. Acc. Chem. Res. 42(8), 1063–1073 (2009). doi:10.1021/ar8002706

26. W. Jian, L. Xuxing, Z. Qiannan, Z. Junwei, S. Qishun, Z. Li, N. Weihai, Angle-resolved plasmonic properties of single gold nanorod dimers. Nano-Micro Lett. 6(4), 372–380 (2014). doi:10.1007/s40820-014-0011-7

27. L. Robert, H. Anming, P. John, Y.N. Zhou, Palladium nanoparti-cles loaded on carbon modified TiO2 nanobelts for enhanced methanol electrooxidation. Nano-Micro Lett. 5(3), 202–212 (2013). doi:10.5101/nml.v5i3.p202-212

28. W. Fagen, X. Yan, Z. Kunfeng, H. Dannong, Preparation of palladium supported on ferric oxide nano-catalysts for carbon monoxide oxidation in low temperature. Nano-Micro Lett. 6(3), 233–241 (2014). doi:10.5101/nml140025a

29. J.J. Pietron, R.M. Stroud, D.R. Rolison, Using three dimensions in catalytic mesoporous nanoarchitectures. Nano Lett. 2(5), 545–549 (2002). doi:10.1021/nl025536s

30. G.A. Somorjai, J.Y. Park, Molecular factors of catalytic selec-tivity. Angew. Chem. Int. Ed. 47(48), 9212–9228 (2008). doi:10.1002/anie.200803181

31. C.H. Liu, B.H. Mao, J. Gao, S. Zhang, X. Gao, Z. Liu, S.T. Lee, X.H. Sun, S.D. Wang, Size-controllable self-assembly of metal nanoparticles on carbon nanostructures in room-temperature ionic liquids by simple sputtering deposition. Carbon 50(8), 3008–3014 (2012). doi:10.1016/j.carbon.2012.02.086

32. C.H. Liu, X.Q. Chen, Y.F. Hu, T.K. Sham, Q.J. Sun, J.B. Chang, X. Gao, X.H. Sun, S.D. Wang, One-pot environmentally friendly approach toward highly catalytically active bimetal-nanoparticle-graphene hybrids. ACS Appl. Mater. Interface 5(11), 5072–5079 (2013). doi:10.1021/am4008853

33. J. Xu, T. White, P. Li, C. He, J. Yu, W. Yuan, Y.-F. Han, Biphasic Pd–Au alloy catalyst for low-temperature co oxidation. JACS 132(30), 10398–10406 (2010). doi:10.1021/ja102617r

34. J.K. Edwards, A.F. Carley, A.A. Herzing, C.J. Kiely, G.J. Hutchings, Direct synthesis of hydrogen peroxide from H2 and O2 using supported Au–Pd catalysts. Faraday Discuss. 138, 225–239 (2008). doi:10.1039/b705915a

35. Y. Mizukoshi, K. Sato, T.J. Konno, N. Masahashi, Dependence of photocatalytic activities upon the structures of Au/Pd bimetallic nanoparticles immobilized on TiO2 surface. Appl. Catal. B: En-viron. 94(3–4), 248–253 (2010). doi:10.1016/j.apcatb.2009.11.015

36. Q. Wang, X. Cui, W. Guan, X. Zhang, C. Liu, T. Xue, H. Wang, W. Zheng, A nanoflower shaped gold-palladium alloy on gra-phene oxide nanosheets with exceptional activity for electro-chemical oxidation of ethanol. Microchim. Acta 181(3–4), 373–380 (2014). doi:10.1007/s00604-013-1119-z

37. T. Pasini, M. Piccinini, M. Blosi, R. Bonelli, S. Albonetti, N. Dimitratos, J.A. Lopez-sanchez, M. Sankar, Q. He, C.J. Kiely, G.J. Hutchings, F. Cavani, Selective oxidation of 5-hydrox-ymethyl-2-furfural using supported gold-copper nanoparticles. Green Chem. 13(8), 2091–2099 (2011). doi:10.1039/c1gc15355b

38. C.-H. Cui, J.-W. Yu, H.-H. Li, M.-R. Gao, H.-W. Liang, S.-H. Yu, Remarkable enhancement of electrocatalytic activity by tuning the interface of Pd–Au bimetallic nanoparticle tubes. ACS Nano 5(5), 4211–4218 (2011). doi:10.1021/nn2010602

39. J. Fang, S.W. Cao, Z. Wang, M.M. Shahjamali, S.C.J. Loo, J. Barber, C. Xue, Mesoporous plasmonic Au–TiO2 nanocompos-ites for efficient visible-light-driven photocatalytic water reduc-tion. Int. J. Hydrog. Energy 37(23), 17853–17861 (2012). doi:10.1016/j.ijhydene.2012.09.023

40. M.C. Long, J.J. Jiang, Y. Li, R.Q. Cao, L.Y. Zhang, W.M. Cai, Effect of gold nanoparticles on the photocatalytic and photo-electrochemical performance of au modified BiVO4. Nano-Micro Lett. 3(3), 171–177 (2011). doi:10.1007/BF03353669

41. M.V. Dozzi, A. Saccomanni, M. Altomare, E. Selli, Photocat-alytic activity of NH4F-doped TiO2 modified by noble metal nanoparticle deposition. Photochem. Photobiol. Sci. 12(4), 595–601 (2013). doi:10.1039/c2pp25175b

42. C. Han, X. Yang, G. Gao, J. Wang, H. Lu, J. Liu, M. Tong, X. Liang, Selective oxidation of methanol to methyl formate on catalysts of Au-Ag alloy nanoparticles supported on titania under UV irradiation. Green Chem. 16(7), 3603–3615 (2014). doi:10.1039/c4gc00367e

43. Y. Wang, J.-M. Zheng, K. Fan, W.-L. Dai, One-pot solvent-free synthesis of sodium benzoate from the oxidation of benzyl al-cohol over novel efficient AuAg/TiO2 catalysts. Green Chem. 13(7), 1644–1647 (2011). doi:10.1039/c1gc15311k

44. A.M. Venezia, V. La parola, G. Deganello, B. Pawelec, J.L.G. Fierro, Synergetic effect of gold in Au/Pd catalysts during hy-drodesulfurization reactions of model compounds. J. Catal. 215(2), 317–325 (2003). doi:10.1016/s0021-9517(03)00005-8

45. P.A.P. Nascente, S.G.C. Decastro, R. Landers, G.G. Kleiman, X-ray photoemission and auger energy shifts in some gold-palladium alloys. Phys. Rev. B **43**(6), 4659–4666 (1991). doi:10.1103/physrevb.43.4659

46. T. Balcha, J.R. Strobl, C. Fowler, P. Dash, R.W.J. Scott, Selective aerobic oxidation of crotyl alcohol using aupd core-shell nanoparticles. ACS Catal. **1**(5), 425–436 (2011). doi:10.1021/cs200040a

47. A. Cybula, J.B. Priebe, M.-M. Pohl, J.W. Sobczak, M. Schneider, A. Zielińska-Jurek, A. Brückner, A. Zaleska, The effect of calcination temperature on structure and photocatalytic properties of Au/Pd nanoparticles supported on TiO₂. Appl. Catal. B: Environ. **152–153**, 202–211 (2014). doi:10.1016/j.apcatb.2014.01.042

48. M.-I. Wu, D.-H. Chen, T.-C. Huang, Synthesis of Au/Pd bimetallic nanoparticles in reverse micelles. Langmuir **17**(13), 3877–3883 (2001). doi:10.1021/la010060y

49. C.H. Cui, H.H. Li, S.H. Yu, A general approach to electrochemical deposition of high quality free-standing noble metal (Pd, Pt, Au, Ag) sub-micron tubes composed of nanoparticles in polar aprotic solvent. Chem. Commun. **46**(6), 940–942 (2010). doi:10.1039/b920705h

50. S. Zhang, Y. Shao, G. Yin, Y. Lin, Electrostatic self-assembly of a Pt-around-Au nanocomposite with high activity towards formic acid oxidation. Angew. Chem. Int. Ed. **49**(12), 2211–2214 (2010). doi:10.1002/anie.200906987

51. V. Ponec, Alloy catalysts: the concepts. Appl. Catal. A: Gen. **222**(1–2), 31–45 (2001). doi:10.1016/s0926-860x(01)00828-6

52. P. Liu, J.K. Norskov, Ligand and ensemble effects in adsorption on alloy surfaces. Phys. Chem. Chem. Phys. **3**(17), 3814–3818 (2001). doi:10.1039/b103525h